First-principles molecular-dynamics simulation of liquid CsPb

de Wijs, G. A.; Pastore, G.; Selloni, A.; van der Lugt, W.

Published in:
Journal of Chemical Physics

DOI:
10.1063/1.470590

Publication date:
1995

First-principles molecular-dynamics simulation of liquid CsPb

G. A. de Wijs, G. Pastore, A. Selloni, and W. van der Lugt

Citation: The Journal of Chemical Physics **103**, 5031 (1995); doi: 10.1063/1.470590
View online: https://doi.org/10.1063/1.470590
View Table of Contents: http://aip.scitation.org/toc/jcp/103/12
Published by the American Institute of Physics

First-principles molecular-dynamics simulation of liquid CsPb

G. A. de Wijs
Laboratorium voor Vaste Stof Fysica, Rijksuniversiteit Groningen, Nijenborgh 4, 9747 AG, Groningen, The Netherlands

G. Pastore
Dipartimento di Fisica Teorica dell' Università, Strada Costiera 11, 34014 Trieste, Italy

A. Selloni
Departement de Chimie Physique, Université de Genève, 30 quai E. Ansermet, CH-1211, Genève, Switzerland

W. van der Lugt
Laboratorium voor Vaste Stof Fysica, Rijksuniversiteit Groningen, Nijenborgh 4, 9747 AG, Groningen, The Netherlands

(Received 23 February 1995; accepted 22 June 1995)

Many alkali–post-transition group IV alloy systems exhibit clearly defined equiatomic compounds together with a pronounced intermediate range ordering, indicated by a first sharp diffraction peak at ≈ 0.9 Å^{-1}. These phenomena have been explained assuming that tetrahedral group IV anions, ''Zintl'' ions, survive in the liquid state. As a prototype system we considered liquid CsPb, for which several experimental results are available, and studied it by means of first-principles molecular-dynamics. Agreement with experiment is satisfactory, provided the $5s$ and $5p$ electrons of cesium are explicitly taken into account in the computation of the electronic valence charge density. In particular, our calculations reproduce the structure factor prepeak reasonably well. The local liquid structure however is quite complex. This can be described as a disordered network, which still has many features in common with the ''Zintl'' ion model. For instance, the average Pb-Pb coordination is close to 3, the value for perfect tetrahedra, but the coordination distribution of Pb around Pb shows a broad range of values. The calculated electronic density of states shows a minimum at the Fermi level indicating compound formation.

I. INTRODUCTION

Liquid alkali–post-transition group IV alloys have been studied extensively during the last decade.[1] Most of these alloys exhibit strong chemical ordering effects that lead to a pronounced intermediate range ordering (IRO). Below we shall concentrate on the alkali-Pb alloys. Without being comprehensive we list the following references 2–8. The alkali-Sn alloys show a behaviour very similar to that of the alkali-Pb alloys.

Resistivity measurements were carried out over almost the whole concentration range from Li-Pb up to and including Cs-Pb.[2–5] It was found that with increasing weight, and consequently size, of the alkali atom the resistivity maximum increases and shifts from the octet (Li-Pb, Na-Pb) to the equiatomic composition (K-Pb, Rb-Pb and Cs-Pb). This effect was explained by Geertsma assuming that Pb_4^{4-} units survive in the liquid state.[9] These so-called Zintl-ions are building blocks of the crystalline compounds NaPb, KPb, RbPb, CsPb (Ref. 7) and many others. Their stability is qualitatively explained as follows: the alkali atoms donate their valence electrons to the more electronegative group IV atoms. In this way the valence configuration of the group IV atoms becomes similar to that of elements in the next column of the periodic table, e.g. P and As. They form a structure similar to the tetrahedra that are formed by P and As in the gas phase: the tetrahedral ''Zintl'' ion: Pb_4^{4-}. With increasing size of the alkali ion the distance between the Pb_4^{4-} units becomes larger. Therefore the bands of the group IV electronic states become narrower and the gap between the occupied bonding and unoccupied antibonding states becomes broader. This is in agreement with the fact that CsPb has the highest resistivity.

The assumption of Zintl ions surviving in the liquid can also explain the occurrence of a prepeak at 0.9 Å^{-1} that is found experimentally in the structure factors of the alloys with heavy alkali atoms.[7] The direct space distance ($\approx 7.7/0.9$ Å) (Ref. 10) corresponding to this prepeak coincides approximately with the shortest distances between the centers of mass of the tetrahedra in the crystal. Molecular-dynamics (MD) simulations, that assume that all Pb are in Pb_4^{4-} tetrahedra with alkali$^+$ ions inbetween, are in fair agreement with the experimental structure factors.[11]

Recently it was found that in CsPb the melting transition is preceded by another transition from the crystalline solid to a plastic phase.[12,13] It was proposed that this plastic phase consists of randomly reorienting Cs_4Pb_4 units on a regular lattice.

Thermodynamic measurements on KPb,[14] NaPb, RbPb and CsPb (Ref. 15) show a remarkable behaviour of the heat capacity (c_P) for the alloys with heavy group IV elements (KPb, RbPb, CsPb). Just above the melting transition the heat capacity is much higher than it is for various other alloys and liquid metals. With the increase of temperature it decreases dramatically. This has been attributed to a rapid disintegration of the clusters as the temperature increases.[15]

So a liquid consisting for 100% of perfect tetrahedra, can at most be expected just above the melting transition.

By contrast, it has been found that the decrease of the prepeak intensity with temperature is very slow.[6,16] In particular, Stolz *et al.*[16] performed measurements on liquid KPb up to 1873 K (60 bar pressure) where they observe that the height of the prepeak has only dropped by about 25%. They also find an increase in the neutron $S(q)$ for very small wavenumbers, suggesting a tendency to phase separation. So the IRO consistent with inter-tetrahedral distances persists to very high temperatures whereas the behaviour of c_P suggests that clusters fall apart rapidly.

The resistivity measurements[2–5] show that as temperature increases the resistivity maximum decreases rapidly but remains at the equiatomic composition. This raises an interesting question: if the clusters, that we assume to be tetrahedra, fall apart, why does the resistivity maximum remain at the equiatomic composition?

The model introduced by Geertsma, in which the Pb atoms are introduced *a priori* as members of tetrahedra, can explain at least qualitatively the occurrence of liquid equiatomic compounds. However, the underlying assumption that just above the melting point all Pb participate in perfect Pb_4 tetrahedra, and the assumption that with increasing temperature they will rapidly fall apart (e.g. $Pb_4^{4-} \rightarrow 4Pb^-$) cannot be tested experimentally. The main reason is that a structure factor yields information on pair correlations only (moreover in the case of a binary alloy like CsPb it is a mix of three partial structure factors). The (partial) information on higher order correlations, implicitly contained in the pair correlations, has been extracted by Howe and McGreevy[17] using the reverse Monte Carlo (RMC) method.[18] However this was insufficient to confirm or reject the model sketched above.

To gain more insight in the chemical bonding and the structural properties associated with it, we carried out a simulation involving no *a priori* notions of the liquid structure and taking into account electronic structure effects (e.g. covalent and ionic bonding). For this study we used the first-principles (FP) Molecular-Dynamics (MD) approach introduced by Car and Parrinello.[19] The FPMD scheme enables a MD on the Born-Oppenheimer (BO) surface, with interatomic forces calculated directly from the instantaneous electronic ground state. This ground state is calculated using density functional theory (DFT) within the local density approximation (LDA).

Similar FPMD studies have been carried out for the liquid alloys NaSn (Ref. 20) and KSi.[21] Experiments[16,22–24] show that Na-Sn is ambiguous w.r.t. compound formation, i.e. there are indications for compounds both near the equiatomic and near the ''octet'' compositions, and exhibits only a weak IRO. Also in Geertsma's model[9] it is a borderline case. Therefore it is not an obvious example system for the study of the liquid ''Zintl''-compounds. According to Geertsma's model KSi and CsPb are suitable example systems. Liquid CsPb has the additional advantage that a variety of experimental data is available[5,7,15] which provides a valuable check on the simulation results.

This paper is organised as follows: The next section mentions the relevant computational details. Section III presents the results on static properties with the exception of the ''inherent structure'' that is presented in Section IV. Next, Section V deals with some dynamical features of the liquid. Section VI covers the electronic properties. Concluding remarks are presented in Section VII. A preliminary account of this work was published elsewhere.[25]

II. SIMULATION METHOD AND TECHNICAL DETAILS

The FPMD method that we use has been described in detail in several references (see, e.g., Refs. 26 and 27). Therefore we shall restrict this discussion to the technical aspects which are relevant for the present simulation.

Our simulation of liquid CsPb was carried out at constant volume [$(15.62\ \text{Å})^3$] using a simple cubic box containing 32 Pb and 32 Cs atoms with periodic boundary conditions (PBC). For the density we took the value from the neutron diffraction experiment[7] at 930 K. The initial configuration was obtained by rescaling the positions of the centers of mass of the Pb and Cs tetrahedra in the orthorhombic crystalline unit cell to the appropriate cubic shape. In this procedure the intratetrahedral distances were not changed. Subsequently the positions were randomised a little, without constraint of the intratetrahedral distances, by an RMC procedure[18] fitting to the experimental $g(r)$.

The electronic states, sampled only at the Γ point of the Brillouin zone (BZ) of our cubic supercell, were expanded in plane waves. For the wave functions the kinetic energy cutoff was 12 Ry, for the pseudo-charge density it was 24 Ry. Electron-ion interactions were described with norm-conserving pseudopotentials. For Pb a scalar relativistic potential from Ref. 28 was employed. For Cs we tried two non-relativistic potentials by Moullet *et al.*[29] First we used the Cs potential with [Xe] core. This potential includes non-linear core corrections.[30] Later we switched to the Cs pseudopotential (PP) with $[\text{Kr}]4d^{10}$ core for reasons explained below. The Kleinman-Bylander (KB) scheme of separable non-locality[31] was used to increase computational speed. Problems related to a ''ghost'' state[32] for Cs were circumvented by using for this element a p reference while including in the calculation s and d non-local terms.[33] For Pb a conventional d reference was employed.

The temperature of the ions in our system was controlled by means of a Nosé[34] thermostat which ensures to obtain correct canonical averages. Another Nosé thermostat was used to keep the electrons close to the ground state, as described in Ref. 35. Moreover, we employed a scheme that reduces the high frequency motion of the electrons[36] by a preconditioning of the fictitious wave function masses. This allowed us to use a time step of 30 a.u. $=7.26\times10^{-4}$ ps. We took $\mu_0=2450$ a.u. for the fictitious mass of the electronic degrees of freedom, and $E_p=1$ Ry for the preconditioning cutoff.

To assess the quality of the pseudopotentials we performed some checks. For fcc Pb we determined the equilibrium lattice constant by means of static total energy calculations. We considered a simple cubic cell with 32 Pb atoms in an fcc configuration, using only the Γ point and the same cutoffs as for liquid CsPb. By variation of the box size we

found a lattice constant of 9.3 ± 0.1 a.u. This is in agreement with the experimental value of 9.35 a.u.[37] To check the influence of the KB scheme we also performed a test using a standard band structure programme without KB. For an equivalent **k**-point sampling and a 12 Ry cutoff we find a lattice constant of 9.19 a.u. Using an extended **k**-point sampling of 10 points in the irreducible part of the BZ the lattice constant decreases slightly to a value of 9.03 a.u. These tests show that the Pb potential suffers little from application of the Kleinman-Bylander scheme and that the cell is of sufficient size for at least the calculation of the lattice constant.

We restrict the discussion of the Cs PP to the PP with $[\mathrm{Kr}]4d^{10}$ core, since all our final results were obtained with this potential. This Cs pseudopotential was successfully used to study CsI under pressure in Refs. 38 and 39. That it can be used in such an ionic environment indicates that the transferability of this pseudopotential is excellent. In Ref. 29 this Cs potential was tested for the dimer and found to reproduce the experimental results well. More particularly relativistic effects are not needed to describe the Cs equilibrium bond length and vibrational frequency to a sufficient degree of accuracy (a few percent). In our tests for this potential we only considered the dimer for kinetic energy cutoffs of 12, 16 and 20 Ry on the wave functions (the cutoffs on the pseudocharge density are twice these values). We found that the equilibrium distance agrees with the experimental data (see e.g. Ref. 29) within a margin of 1 percent.

In our preparation of the liquid sample, initially the Cs pseudopotential with [Xe] core was used. After a period of equilibration (4 ps) a strong tendency to phase separation became apparent in that the partial structure factor for lead, S_{PbPb}, became very large in the region below $q=1$ Å^{-1}. We continued for another 4 ps but the tendency to phase separation became even stronger. Subsequently we went back to a point in our simulation where Pb was still more or less evenly distributed over the simulation cell (3 ps since the beginning) and continued our simulation from there using the Cs pseudopotential with $[\mathrm{Kr}]4d^{10}$ core. During these 3 ps we had equilibrated the liquid at approximately 1000 K above the experimental melting point. Then, in a period of 4.6 ps, we cooled from 2000 K to 1050 K. At 1050 K we restarted the Nosé particles and allowed the system to relax for another 5.1 ps. (The Nosé masses were 10 000 000 and 250 a.u. for atoms and electrons respectively.) Finally statistics was collected for 10.8 ps. Since there was a slight tendency for the Cs to be on average "hotter" than the Pb, during the last 2.9 ps we used two Nosé particles, one for Cs and one Pb, instead of just one controlling the average temperature of Cs and Pb together.

III. STATIC PROPERTIES

First we will consider the liquid structure in direct space. In Fig. 1 we show the radial distribution function $N(r)$ (see e.g. Ref. 7) from experiment and our simulation. There is a fair agreement between experiment and simulation. The first peak is well resolved. After the first peak the experimental data from Reijers *et al.*[7] show two clear maxima (3.8 and 4.4 Å) followed by a faint peak (5.0 Å) before the steep rise. The experimental data by Price *et al.*[8] show, in the same region,

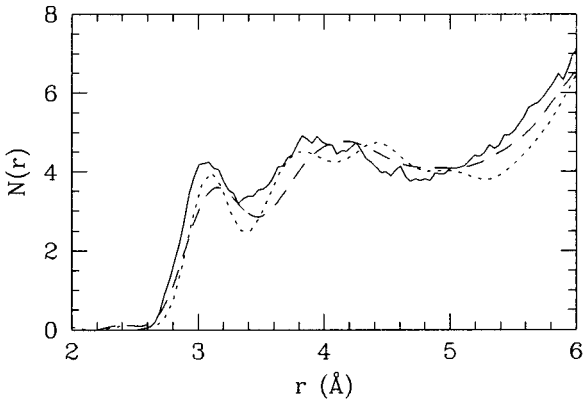

FIG. 1. $N(r)$ compared with experiment. Simulation at 1050 K: continuous line. Experiment from Ref. 7 at 930 K: dotted line. Experiment from Ref. 8 at 933 K: dashed line. In the construction of the $N(r)$ from Ref. 8 the density from Ref. 7 was used. We used a scheme from Ref. 55 to calculate the pair distribution functions beyond half of the length of the simulation box.

only one broad peak. We find also one broad peak in this region, however it is shifted with respect to Price's data. Inspection of the partial pair correlation functions g_{ij} in Fig. 2 indicates that this broad peak essentially consists of a Cs-Pb and a weak Cs-Cs peak. In the interval from 5 to 6 Å the agreement with Price *et al.* appears to be better. However Price's curve may be a little biased since in reconstructing it from $D(r)$ (see e.g. Ref. 7) we used the density from Reijers *et al.*

In Fig. 2 the partial pair distribution functions g_{ij} are shown. Note the relative order of the coordination shells. $g_{\mathrm{Pb-Pb}}$ has a narrow high peak with a maximum at 3.0 Å, followed by a deep minimum around 4.5 Å, and, hardly visible, a very broad peak. The Cs-Pb coordination shell is less

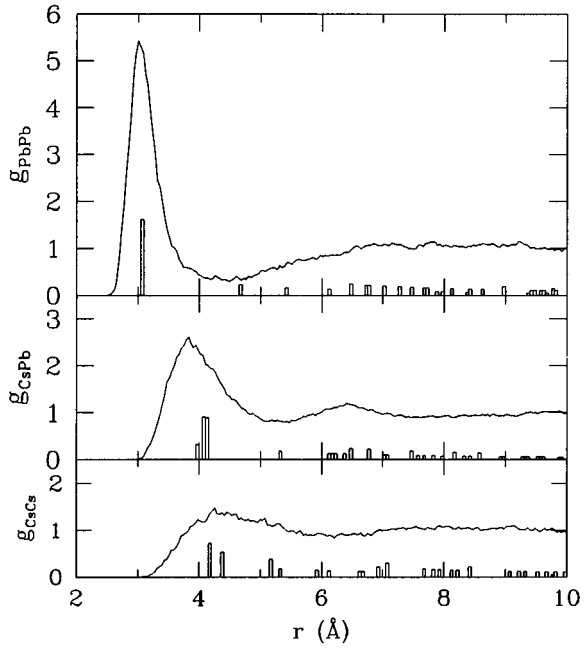

FIG. 2. Partial pair distribution functions. The "histograms" are proportional to the solid state g_{ij}.

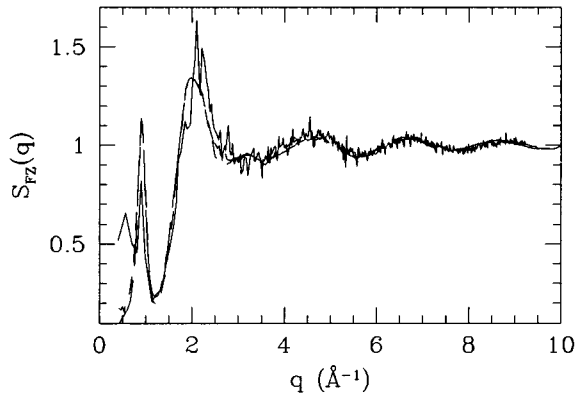

FIG. 3. Faber-Ziman $S(q)$ compared with experiment. Simulation at 1050 K: continuous line. Experiment from Ref. 7 at 930 K: short dash. Experiment from Ref. 8 at 933 K: long dash. Both experimental curves coincide. Only just beyond the main peak (2.5-3 Å^{-1}) they slighty differ.

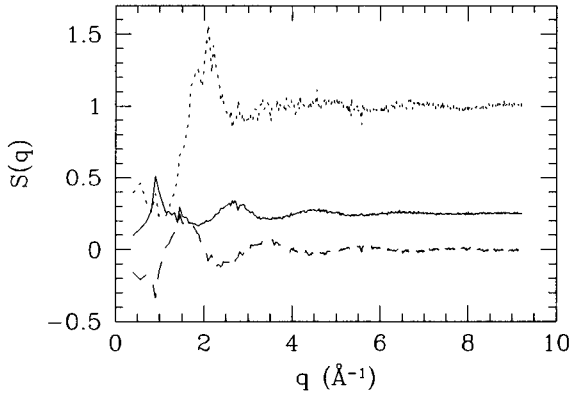

FIG. 5. Bhatia-Thornton partial structure factors. Continuous line: S_{CC}, dotted line: S_{NN}, dashed: S_{NC}.

well defined, since after the first peak there is only a shallow minimum. We extract the following coordination numbers: 3.3 (PbPb), 6.7 (CsCs) and 5.1 (CsPb). These numbers were obtained by integration up to cutoffs of 4.1, 6.0 and 5.0 Å respectively.

Now we move to the structure in reciprocal space. The structure factor $S(q)$, according to the Faber-Ziman definition, is shown in Fig. 3. Note that on the scale of the plot the difference between the two experiments[7,8] is discernible only just after the main peak. Beyond 4.5 Å^{-1} our simulation agrees very well with experiment. The tiny peak at $\approx$3.2 Å^{-1} is not well resolved by the simulation as it is almost of the size of the numerical noise. At the top of the main peak there is a shift of about 7 %, whereas the rise of the peak from the minimum at 1.2 Å^{-1} and the minimum itself are very accurately reproduced. The prepeak is found exactly at the experimental position, but its height is underestimated by about 25 %. In the region before the prepeak our calculated $S(q)$ is too high with respect to experiments.

The partial Ashcroft-Langreth structure factors S_{ij} are displayed in Fig. 4. The ordering of the main peaks reflects the size difference of the constituents. S_{Cs-Cs} has very little structure: it rises from almost 0, with a small shoulder, to the top of the main peak. Beyond this peak essentially $S_{Cs-Cs}=1$. S_{Cs-Pb} and S_{Pb-Pb} show much more structure. They both have a prepeak at 0.9 Å^{-1}. This reflects an IRO for the Pb atoms. The prepeak in S_{Cs-Pb} is likely to originate from the Cs occupying the empty space between the clusters of Pb atoms. The IRO is reflected in S_{Cs-Cs} only by the shoulder in the rise of the main peak. Note that in the very low q region S_{Pb-Pb} is rather high: this is the origin of the discrepancy with experiments at very low q's for the total $S(q)$.

In Fig. 5 the Bhatia-Thornton[40] structure factors are presented. In the prepeak region the concentration (C) and number (N) fluctuations clearly correlate. S_{CC} exhibits a quite large prepeak. The discrepancy in the very low q region ($q<0.9$ Å) between the total $S(q)$ as obtained from experiment and that obtained from simulation originates from S_{NN} and S_{NC}. In S_{NN} an increase for q going to 0 is clearly present, suggesting either that the box size (15.62 Å^3) does not match the periodicity of the IRO associated with the prepeak or that the density of our sample is not entirely correct.

The bond angle distributions are displayed in Fig. 6. Most prominent is the peak in b_{PbPbPb} around 60° (actually the maximum is reached at 57°, it slightly varies with cutoff) in Fig. 6a. This is a clear remnant of the Pb_4 tetrahedra in the

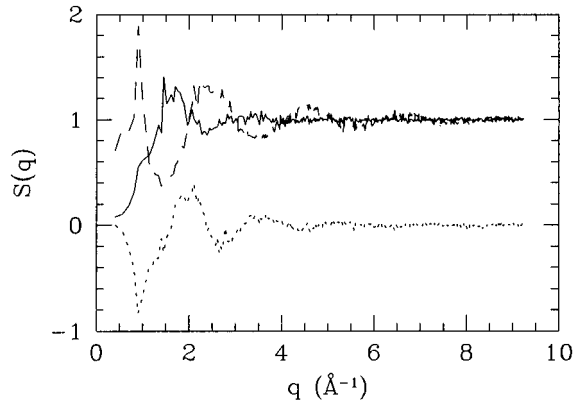

FIG. 4. Ashcroft-Langreth partial structure factors. Continuous line: S_{Cs-Cs}, dotted line: S_{Cs-Pb}, dashed: S_{Pb-Pb}.

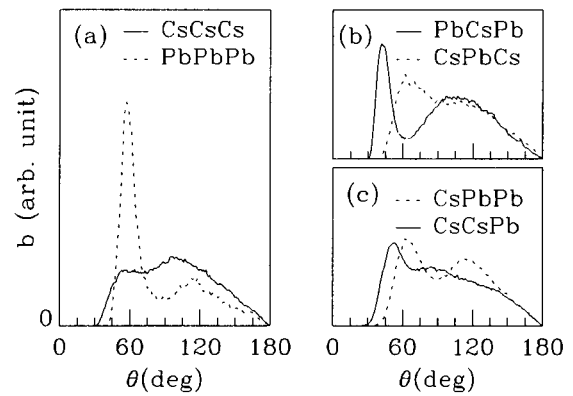

FIG. 6. Bond angle distributions. Cutoff distances are 4.0, 5.0, and 6.0 Å for PbPb, CsPb and CsCs distances respectively.

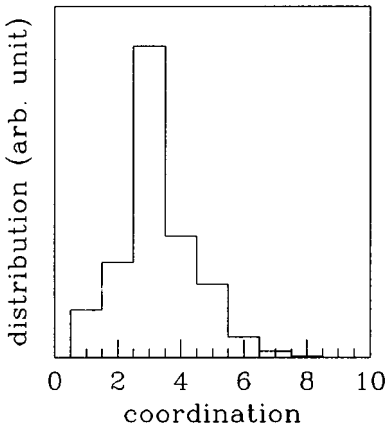

FIG. 7. Pb coordination distribution, cutoff distance: 4.0 Å.

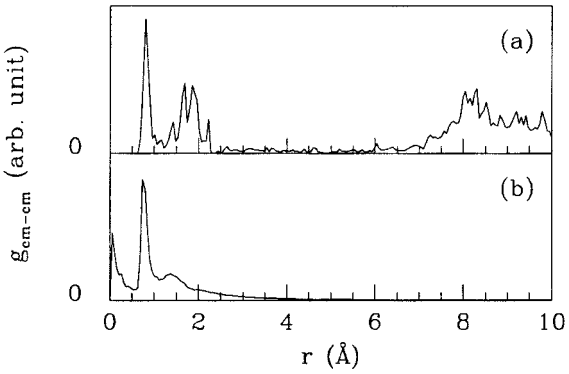

FIG. 8. Pair distribution function of the center of mass of the distorted tetrahedral units, not normalised. Figures a and b are according to definitions 1 and 2 respectively.

solid state. Around 120° an additional maximum can be seen, separated by a minimum at 90° from the main peak. Considering the shape of g_{PbPb} (sharp peak, deep minimum, slow increase to 1) these features are not surprising. In contrast, b_{CsCsCs} shows only a weak deviation from the ideal $\sin(\theta)$ behaviour.

In Fig. 6b b_{PbCsPb} and b_{CsPbCs} are compared. The considerable difference between Cs and Pb "atomic" sizes is reflected by the positions of the main peaks (Fig. 2). The shape and positions of the first peaks in b_{PbCsPb} and b_{CsPbCs} are consistent with the shape and positions of the peaks of the g_{PbPb} and g_{CsCs} that represent the first coordination shells: e.g. the sharp peak followed by a deep minimum in g_{PbPb} is clearly mirrored by the features of the same shape in b_{PbCsPb}. The opposite holds for g_{CsCs} and b_{CsPbCs}. Similarly, the relative positions of the first peaks in the distribution of the CsCsPb and CsPbPb bond angles (see Fig. 6c) reflect the size difference between Cs and Pb.

Already from the bond angle distribution b_{PbPbPb} it emerges that there are not only perfect tetrahedra in the liquid. In fact most of the isolated tetrahedra are found to be destroyed as such and a much more complex structure is present. Below we try to characterise this structure in terms of some statistical quantities in a similar fashion as has been done for liquid KSi.[21] This enables us also to make a comparison between liquid CsPb and liquid KSi.

First we remark that the most obvious 4-body correlation function, the dihedral angle distribution, in case of perfect tetrahedra should have two peaks: at 0° and at 70.5°. Instead, the dihedral angle distribution that we obtain from our simulation shows no structure at all when averaged over the duration of the run (we do not give a plot of this function since we do not consider its statistical quality to be sufficient).

The average coordination of Pb around Pb, already mentioned above, is 3.3, a value very near that of tetrahedra. The coordination distribution of Pb around Pb (Fig. 7) however shows a broad range of realised coordinations, with a maximum at 3.

Next we consider the correlations between the remnants of the tetrahedra. In order to do so a definition of "a remnant of a tetrahedron," a "distorted tetrahedral unit" (DTU), is needed. Two possible definitions are proposed below:

(1) A DTU is defined as a threefold coordinated Pb (cutoff distance 4.0 Å) together with its three neighbouring Pb atoms. This definition of a DTU is also used in Ref. 21 for distorted Si tetrahedra in liquid KSi. Note that this definition is biased in two ways. A DTU that is in shape more similar to a tetrahedron is counted more often: e.g. an ideal tetrahedron is counted 4 times. If a DTU with its 3 fold coordinated Pb gets linked to another Pb it will not be counted anymore (since now the Pb is not 3 fold coordinated anymore). So isolated DTU have higher statistical weight than those connected to other Pb.

(2) A DTU is defined as a set of 4 Pb atoms of which at least one has all the other Pb in its first coordination shell (again we take a cutoff distance of 4 Å). In this definition all DTU have equal statistical weight, irrespective of their surroundings and shape.

From these definitions it already transpires that in interpreting the correlation functions of DTU's care is required. For the DTU's, according to the above definitions, the pair correlation function ($g_{\mathrm{cm-cm}}$) of their centers of mass (cm) and the distribution (N_{VOL}) of their volume are shown in Figs. 8 and 9 respectively. The volume of a DTU is defined as the

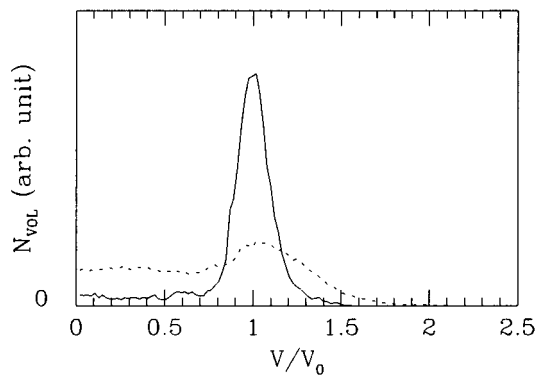

FIG. 9. Volume distribution of distorted tetrahedral units. The continuous and dashed lines are according to definitions 1 and 2 respectively. $V_0=3.5$ Å^3.

volume of the ''distorted'' tetrahedron that has its vertices at the nulcei of the Pb atoms of the DTU.

Both N_{VOL} and $g_{\mathrm{cm-cm}}$, calculated according to definition 1, are very similar to those for the KSi case. The volume of a tetrahedron in the CsPb crystal (V_0) is: 3.5 Å^3 (for a perfect tetrahedron with interatomic distance 3.1 Å). N_{VOL} is sharply peaked around this volume; i.e. the distorted tetrahedra are quite similar in size to the solid state ones. The short range part of $g_{\mathrm{cm-cm}}$ shows that tetrahedra are linked to each other in various ways. During the run the values of $g_{\mathrm{cm-cm}}$ below a distance of 2.5 Å were found to decrease until almost zero, whereas at the end of the run a little increase was observed again. Evidently the statistics for $g_{\mathrm{cm-cm}}$ in this range is not very reliable. In $g_{\mathrm{cm-cm}}$, starting at 8 Å, a remnant of the inter-tetrahedral correlations from the crystalline phase appears. It corresponds to the prepeak in $S(q)$ at 0.9 Å^{-1}: the direct space distance associated with this peak is $7.7/0.9 = 8.6$ Å. This feature of $g_{\mathrm{cm-cm}}$ is stable over the duration of the run.

Definition 2 puts emphasis on other features. In N_{VOL} there is a plateau at small values of the volume; not only tetrahedral-like Pb arrangements are present but also geometries yielding a whole range of small volumes, extending even to planar arrangements. Note that the tetrahedral volume is still slightly favoured. Some vague structure persists in $g_{\mathrm{cm-cm}}$ around 8 Å, but on the scale of the plot it is not visible. The statistics in the region below 2.5 Å is much better for definition 2. The clear peak at 0.75 Å is due to face sharing DTU's.

The two definitions clearly put emphasis on different aspects of the system. Since these definitions provide, each in its own way, a restricted view on the system, one may wonder how reliable the information conveyed by N_{VOL} and $g_{\mathrm{cm-cm}}$ actually is. Snapshots of the configurations, taken at various moments during the run, (e.g. Fig. 10) confirm the picture that has arisen from the correlation functions of the DTU's. From the snapshots it emerges that one large extended Pb cluster is present from which occasionally some clusters are split off. We find that during the 10.8 ps time window of observation, there are distinct tetrahedra that split off from and/or become linked to the large cluster for a short while. There are 2 tetrahedra (a cutoff distance for Pb bonds of 4 Å was applied) that are essentially stable over the whole run, but sometimes are linked to each other or to the extended cluster. A third isolated tetrahedron exists for 2 to 3 ps.

Furthermore, still using a cutoff distance of 4 Å, we found that only even membered clusters occur during our statistics run. Apart from the tetrahedra that we already mentioned, we found a dimer, a dimer linked to a tetrahedron and 2 tetrahedra linked together. These structures occur far less often than the tetrahedra. Since they occur so less frequently we have insufficient statistics to claim that odd membered clusters do not exist. This point deserves a further investigation: assuming a formal charge transfer of one electron to each Pb, even membered Pb clusters are a necessity if no clusters are allowed to have half filled electron states.

The shape of the large cluster is of course much affected by the periodic boundary conditions (occasionally it is linked to its periodic image), but it can be seen to consist of strings and triangles that favour a tetrahedral geometry. One part of the extended cluster is quite compact, consisting of face-sharing DTU's (definition 2).

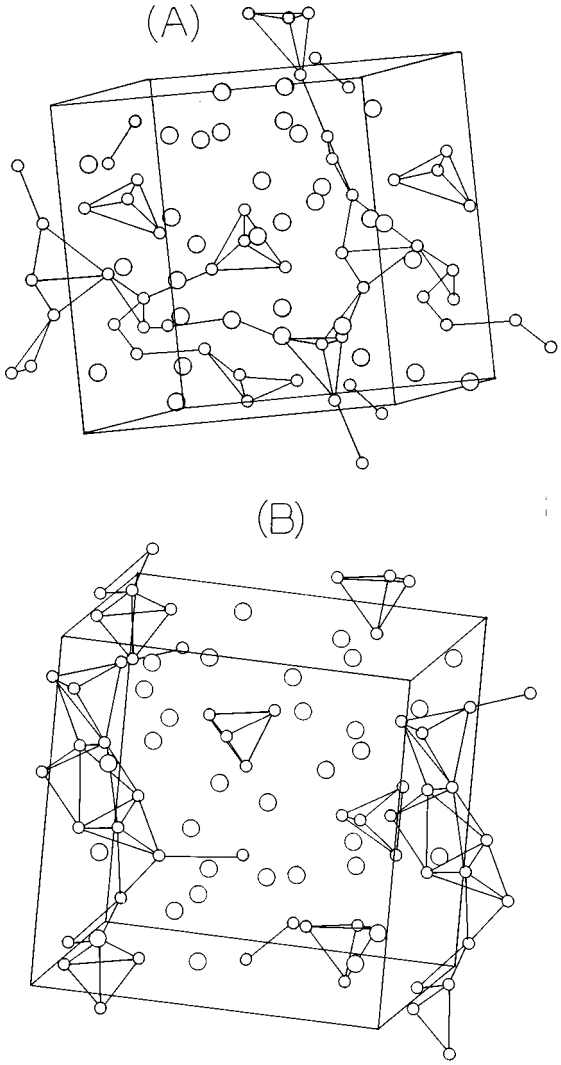

FIG. 10. Two snapshots of configurations during the simulation. The Pb atoms are shown as small solid spheres, the Cs atoms as large ones. Bonds between the Pb are drawn if the distance between them does not exceed 4.0 Å. The boxes shown have the size of the simulation cell. In picture (a) one is looking slightly from the bottom and from the left to such a box. In picture (b) one is looking from above and from the right. All Pb and Cs atoms in the box are shown (32 atoms each) and some of the Pb atoms outside the box that are either directly or indirectly ''bonded'' to the Pb atoms insided the box. There is no perspective in the plots, i.e. the observer is at ''infinite'' distance.

IV. INHERENT STRUCTURE

Inspired by the work of Stillinger and Weber[41,42] on 2 dimensional liquids we set out a search for local minima on the BO surface whose basins of attraction in the configuration space are visited by our liquid. The resulting atomic configurations are called the inherent structure. A steepest descent (SD) algorithm is rather inefficient in locating these minima. Instead we employed a damped second-order dynamics, i.e.:

$$M_I\ddot{\boldsymbol{R}}_I = -\nabla_{\boldsymbol{R}_I} E_{\mathrm{KS}} - \gamma M_I \dot{\boldsymbol{R}}_I , \tag{4.1}$$

where R_I and M_I denote the atomic positions and masses respectively, E_{KS} denotes the Kohm-Sham energy functional and γ stands for the damping coefficient. Such a damped second-order dynamics was introduced in Ref. 36 for energy minimisation w.r.t. the electronic degrees of freedom, we however employ it for the ionic motion only. In order to maximise the rate of convergence, the damping coefficient γ should be chosen as small as possible without making the motion oscillatory: i.e. the system should be critically damped. Since the frequencies of the ions go down to a minimum of 0, this condition can in principle not be realised. We tried several values of γ and consider 7.5×10^{-5} a.u. the best choice for our system. In parallel to the damped dynamics of the ions, the electrons evolved like during the MD simulation with the difference that no thermostat was applied, i.e. by means of an un-damped second-order dynamics. Consequently, after some time, the electrons will move from the BO surface. Therefore we occasionally bring the electrons back to their ground state by means of a SD while momentarily stopping the ionic motion. After an SD the fictitious electronic dynamics is restarted with almost zero velocity.

We experienced that, in the vicinity of a local minimum, the curvature of the BO surface is very small. A complete convergence becomes extremely costly and therefore is not feasible. We stopped our damped dynamics when we did not observe a significant decrease of E_{KS} anymore. Averaged over the three starting configurations, at 3.6 ps intervals, we found a decrease of the total energy of 0.27 eV per Pb atom.

Since the computational cost of these runs is rather high we considered only 3 configurations. Because of the limited statistics we will restrict the discussion to qualitative statements only. We find that the features in the g_{ij} become sharper once the thermal vibrations have been quenched out. g_{PbPb} peaks very sharply at a distance of 3.05 ± 0.05 Å: the equilibrium bond length in the system. Also the g_{CsPb} first peak significantly sharpens. For g_{CsCs}, like for g_{CsPb}, the shortest distances become longer, but the numerical noise prevents saying anything about a possible sharpening of the peak. With a cutoff of 3.25 Å for Pb-Pb distances, which just includes the sharp peak at 3.05 Å, we looked at the sizes of the Pb clusters. The modification of the bonds is found to have little effect on the cluster distribution and topology. The large cluster, described in the previous section, is essentially not affected by the quenching. Apart from this large cluster we only find a few four-membered clusters. Using again a cutoff of 4 Å, we only see a few Pb-Pb bonds that break (about 2) or come into existence (about 3).

Since the g_{PbPb} for the inherent structure is quite sharply peaked we can make a reasonably accurate count of the bonds. We define a Pb-Pb bond by means of a cutoff length. If we assume that all Pb-Pb bonds are simple covalent bonds (the two bonded atoms share one pair of electrons) we can calculate the number of electrons that on average needs to be transferred to a Pb to fill its valence shell. For a cutoff of 3.25 Å this is about 1.4 electron, for a cutoff of 3.5 Å it is 1.0 electron. Although the sensitivity to the cutoff radius remains rather large, the numbers are quite reasonable.

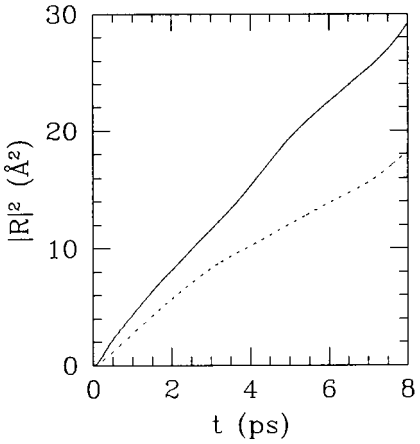

FIG. 11. Mean squared displacement as a function of time. Continuous line: Cs, dotted line: Pb.

V. DYNAMIC PROPERTIES

The mean squared displacement for both atomic species is shown in Fig. 11. The diffusion coefficients were calculated from a least squares fit to the mean squared displacement via the Einstein relation. The fitting range was from 1.0 to 5.0 and from 0.5 to 2.5 ps for Cs and Pb respectively. The following diffusion coefficients were obtained: $D_{\mathrm{Cs}}=6\times10^{-5}\mathrm{cm}^2/\mathrm{s}$ and $D_{\mathrm{Pb}}=5\times10^{-5}\mathrm{cm}^2/\mathrm{s}$. The ratio $D_{\mathrm{Cs}}/D_{\mathrm{Pb}}$ is close to what can be expected considering the mass ratio only.

Figure 12a shows $Z(t)$, the velocity auto correlation function (VACF), for both species. A caging shows up for the Cs atoms, but not for Pb atoms. The spectral density of the VACF,

$$\mathcal{Z}(f)\sim\int_0^\infty Z(t)\cos(2\pi f t)\,\mathrm{d}t, \tag{5.1}$$

is given in Fig. 12b. For Cs it is rather unstructured but for Pb a shoulder at about 2.2 THz occurs. The other ripples are noise due to insufficient statistics, perhaps with the exception of the slight shoulder in $\mathcal{Z}_{\mathrm{Pb}}$ at 3.8 THz. We cut the integra-

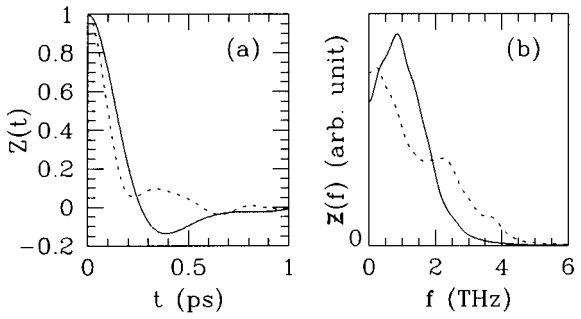

FIG. 12. (a) Velocity auto correlation functions. (b) Spectral density of the VACFs. Continuous line: Cs, dotted line: Pb.

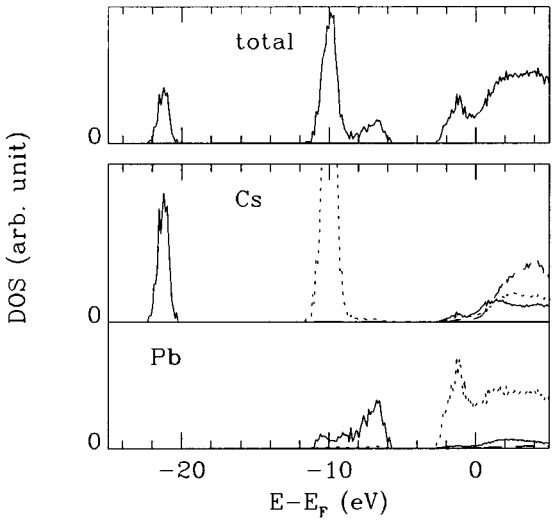

FIG. 13. Electronic densities of states, obtained by averaging over 10 liquid configurations generated during our MD run. The top panel shows the total DOS, the lower panels show its decomposition into Cs and Pb contribution of various angular momenta. (s: continuous line, p: dotted line, d: dashed line). E_F denotes the Fermi level. Note that the DOS-axis scale in the upper panel is different from that in the lower panels.

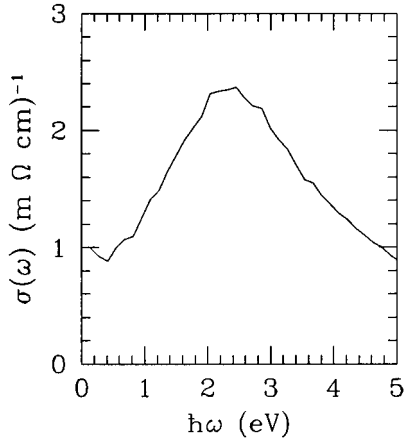

FIG. 14. Frequency dependent conductivity. It was obtained from the same data as the DOS, via the Kubo-Greenwood formula.

tion at 3.6 ps and applied a 4-term Blackman-Harris window function[43] to correct for the abruptness of the cut. The diffusion coefficients extracted from $\mathscr{Z}(0)$, i.e. $D_i=(k_{\mathrm{Boltz}}T/M_i)\int_0^\infty Z_i(t)\mathrm{d}t$, are in fair agreement with those calculated by the Einstein route.

In the case of KSi, Galli and Parrinello[21] attribute a feature in $\mathscr{Z}_{\mathrm{Si}}$, similar to the shoulder at 2.2 THz in $\mathscr{Z}_{Pb}(f)$, to the presence of Zintl-type anion complexes (Si_4^{4-}). In the present case such an assignment is not unambiguous: the ground state frequency of the Bi_2 (Pb^- is isoelectronic to Bi) molecule is 5.1 THz whereas the excited states have slightly smaller frequencies[44] and Bi_4, very likely to be a tetrahedron, has frequencies in the range 2.5–4.5 THz.[45] Furthermore, for the analogous case of Si and P it has been observed that the frequencies of Si_4^{4-} are about 20% smaller than those of P_4.[46,47]

VI. ELECTRONIC PROPERTIES

The total and partial density of states (DOS) (see Fig. 13) were obtained by averaging over 10 configurations sampled at constant time intervals during the 10.8 ps of our production run. The excited states were constructed using the self-consistent (Hartree and exchange-correlation) potential for the occupied states. The angular momentum decomposition was obtained by projecting on spherical harmonics within spheres of radius 1.59 Å.

The Cs 5s states are located below -20 eV. The large peak at -10 eV originates from the Cs 5p states. Quite close to this, peaking at -7 eV, the Pb 6s states are found. They have a tail that overlaps the Cs 5p states: so these Cs states are not chemically inert but tend to hybridise with the Pb 6s states.

Just below the Fermi level the states are almost completely of Pb p character. A minimum, but not a gap, is observed at the Fermi level. The rise in the DOS above the Fermi energy (E_F) is mostly due to Cs states (note the large d contribution). Also note that states with s and p symmetry on the Pb atoms are energetically well separated. For the tetrahedral P_4 molecule (Pb^- is isoelectronic to P) Hart *et al.*[48] also find very little $s-p$ hybridisation.

It is interesting to compare the DOS of CsPb to the DOS, also calculated using the LDA, of the crystalline compounds NaSn (Ref. 49) and KPb.[50] The densities of states of these solid compounds are very similar; on the group IV atoms both have, going from low to high energy, two s type bands and a p type valence band, separated by a gap (resp. ≈ 0.3 eV and ≈ 0.5 eV) from a p type conduction band. The splitting into 3 valence bands is reminiscent of the term scheme of P_4. In our liquid the gap is replaced by a minimum; the two s bands merge into one broad band.

The frequency (ω) dependence of the conductivity (σ) was obtained from the Kubo-Greenwood formula,[51] using the same data as used for the construction of the DOS. We calculated $\sigma(\omega)$ by applying a Fermi distribution both at zero temperature and at the temperature of the simulation (1050 K). We found the difference, even at the lowest frequencies, to be negligible. Figure 14 shows the curve for the step-like Fermi distribution. Extrapolating to zero frequency, we find for the DC conductivity a value of 0.9 (m Ω cm)$^{-1}$. Extrapolating[52] the experimental conductivity data[5] to the simulation temperature of 1050 K yields 1 (m Ω cm)$^{-1}$. Note that just above the melting transition values of 0.16 (m Ω cm)$^{-1}$ have been observed.[5]

The participation ratio,

$$P_i=\left(\Omega\int_\Omega \mathrm{d}\boldsymbol{r}\,|\psi_i(\boldsymbol{r})|^4\right)^{-1}, \tag{6.1}$$

where ψ_i is normalised and Ω is the volume of the system, yields information on the degree of localisation of the states ψ_i (see e.g. Ref. 53). Its upper bound, reached for plane waves $[(1/\sqrt{\Omega})]\mathrm{e}^{\mathrm{i}kr}$), is 1. For states occupying only a volume V it will be approximately V/Ω. In real liquid systems Ω will go to infinity and thus for localised states $P_i\rightarrow 0$.

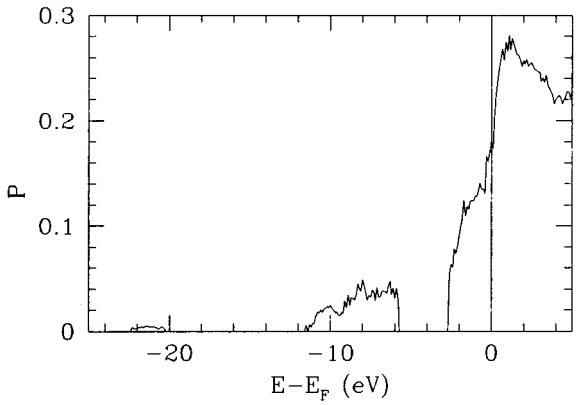

FIG. 15. Participation ratio. Shown is a histogram of the average participation ratio as a function of energy. It was obtained from the same data as the DOS. $\Omega = 3809 Å^3$.

From our results (see Fig. 15), it appears that P takes on considerable values for states just below (in a range of a few eV) the Fermi level. Around the Fermi level it jumps to even higher values (up to almost 0.3), followed by a gradual decrease. One can extract some rough indication on the extension of the wave functions by inverting equation 6.1 and assuming the electron in state ψ_i to be uniformly distributed over a spherical region where ψ_i is non-zero. In this way we obtain for the radii of the states: 1.6 Å for the Cs 5*s* states ($P=0.005$), 3.2 Å for the Pb 6*s* states ($P=0.035$), 4.5 Å at the onset of the Pb 6*p* states ($P=0.1$) and 5.4 Å at the Fermi level ($P=0.175$). Considering the fact that one should view these numbers as a lower limit on the spatial extension of states, the mixing of Cs 5*p* and Pb 6*s* states does not come as a surprise.

The shortest distance between two Pb atoms on different tetrahedra (assuming a model in which prefect tetrahedra can rotate freely, with their centers of mass fixed at a distance corresponding to the experimental prepeak position: 7.7/0.9 =8.6 Å) is 5.5 Å. Note that half of this distance is significantly less than the tentative radius of almost all the Pb 6*p* states. This means that even if all Pb were in tetrahedra, the extension of the Pb states in our model would allow electrons to wander from tetrahedron to tetrahedron.

It is well known that DFT generally has problems in correctly describing energy levels. In particular it is known that it tends to underestimate energy gaps between occupied and empty states. In our case, this may lead us to an overestimation of the conductivity. Since we cannot very accurately define the thermodynamic state of our sample (w.r.t. its melting transition) the good agreement we find with the extrapolation of the experimental resistivity data is partly fortuitous. Another complication is that temperature effects become noticeable in a very narrow energy range of a few $k_{\mathrm{Boltz}}T$ that is comparable to the resolution of the calculated $\sigma(\omega)$.

VII. CONCLUDING REMARKS

In this last section we like to make a few remarks and comments concerning the comparison of our results with experiments. We first remark that our simulation was carried out at 1150 K, while the neutron-scattering experiments were performed just above the liquidus at a temperature of 930 K.[7,8] Because we employ an approximate theory, the melting point of the simulated sample will not coincide exactly with the experimental value. A deviation of some tens of Kelvins is possible. The location by means of computer simulation of the melting transition, from the *plastic* to the liquid phase, is a formidable task that we did not carry out. By simulating at a temperature a little over 100 K above the experimental melting temperature we ensured that we obtained a liquid sample. Another related reason for not setting a lower temperature in the simulation is that this would slow down the atomic motion, thus requiring even longer simulation times.

In view of the above and the fact that experimentally the resistivity is found to decay strongly as temperature increases[5] a detailed comparison with experiment is very difficult. The comparison to the experimental $S(q)$ is much less problematic: in the related liquid alloy KPb experiments prove that the diminution of the prepeak with temperature is rather slow.[16]

Another delicate point is the size of the simulation cell. With all Pb atoms arranged in tetrahedra, each tetrahedron finds in its first coordination shell all its nearest neighbour tetrahedra twice. This may cause a serious bias on the freedom of the tetrahedra to adapt themselves to their surroundings.

Despite all the above limitations we can still extract meaningful information from our simulation results.

It was already noted that the chemical ordering is not much affected by the PBC: there is no extra peak or increase of S_{CC} before the prepeak (Fig. 5).

Our results show that the states just below the Fermi level are almost entirely of *p* symmetry, at E_{F} there is a jump in the participation ratio and a minimum in the DOS. These features are qualitatively in accordance with the Geertsma model. Comparing to the KSi simulation[21] a trend can be seen. Both compounds are well inside the clustering region in Geertsma's stability diagram.[9] KSi is at the bottom of the II^{B} region whereas CsPb, and all the other alkali-Pb compounds, are located much closer to region II^{A}. So the bonding–antibonding splitting should be much stronger for KSi. Indeed in the case of KSi a much deeper DOS minimum at E_{F} is observed in the simulation.

A most intriguing aspect of the behaviour of the clustering alkali-group IV liquid alloys is that with the rise of temperature their stoichiometry remains at the equiatomic composition. Geertsma's model of the equiatomic liquid, consisting of perfect tetrahedra, can account for the occurrence of a gap at E_{F}. Thus it provides a good indication for the existence of an equiatomic compound. However the rapid decrease of e.g. c_P with temperature[15] shows that some kind of dissociation process of the clusters must take place. Then there is no simple explanation anymore for the gap to occur at E_{F}, and consequently no reason why a compound still exists at the 50-50 composition.

We find that in a liquid with Pb participating in a complex network still a minimum in the DOS at E_{F} is formed and that the participation ratio jumps almost exactly at E_{F}. These facts are indications that we are still dealing with a stoichiometric composition. The Pb assemble in complicated

non-symmetric structures, reminiscent of tetrahedra in many ways, still exhibiting a significant degree of IRO as demonstrated by the presence of a prepeak. For liquid KSi a similar effect was found. In our case the good overall agreement with the neutron scattering experiments gives confidence that no questionable approximations have been made.

Of course simulation data at other compositions would be desirable. In view of the very high computational cost we did not attempt a simulation at another composition. Most interesting would be the Cs-rich compositions where a tendency to phase separation is observed.[8]

In the Introduction we already mentioned the somewhat paradoxical situation that neutron scattering experiments suggest that the IRO persists to very high temperatures[16] but that thermodynamic measurements (c_P) suggest a very rapid dissociation of the poly-anions.[15]

On the basis of Ref. 16 and in line with our simulation one may speculate that with the increase of temperature the Pb atoms tend to leave the tetrahedral conformations. They form more extended clusters, partly build up of DTU's. The electronic structure is qualitatively not different of that of the perfect Pb_4 unit. These extended clusters are more metallic and may form percolating structures which provide paths for an easy conduction of electrons. The extended clusters show up as concentration fluctuations in the low q limit. Note that in this picture the Pb-Pb bonds do not break but only rearrange. The dramatic behaviour of c_P needs closer investigation.

ACKNOWLEDGMENTS

We acknowledge useful discussions with Dr. W. Geertsma and Professor J. Th. M. de Hosson. We thank Dr. W. Andreoni, Dr. P. Giannozzi and Dr. I. Garzon for useful information and help in using the Cs pseudopotential. We thank Dr. D. L. Price and Dr. M. L. Saboungi for providing us with tables of their experimental results. Calculations were carried out on the Cray Y-MP4/64 and Cray C98/4256 of SARA at Amsterdam (The Netherlands) and on the Nec-SX3 of the CSCS at Manno (Switzerland). This work was sponsored by the Stichting Nationale Computerfaciliteiten (National Computing Facilities Foundation, NCF) for the use of supercomputer facilities, with financial support from the Nederlandse Organisatie voor Wetenschappelijk Onderzoek (Netherlands Organisation for Scientific Research, NWO).

[1] W. van der Lugt, Phys. Scr. **T39**, 372 (1991).
[2] V. T. Nguyen and E. Enderby, Philos. Mag. **35**, 1013 (1977).
[3] C. van der Marel, A. B. van Oosten, W. Geertsma, and W. van der Lugt, J. Phys. F **12**, 2349 (1982).
[4] J. A. Meijer, W. Geertsma, and W. van der Lugt, J. Phys. F **15**, 899 (1985).
[5] J. A. Meijer, G. B. J. Vinke, and W. van der Lugt, J. Phys. F **16**, 845 (1986).
[6] M.-L. Saboungi, R. Blomquist, K. J. Volin, and D. L. Price, J. Chem. Phys. **87**, 2278 (1987).
[7] H. T. J. Reijers, M.-L. Saboungi, D. L. Price, J. W. Richardson Jr., K. J. Volin, and W. van der Lugt, Phys. Rev. B **40**, 6018 (1989).
[8] D. L. Price, M.-L. Saboungi, G. A. de Wijs, and W. van der Lugt, J. Non-Cryst. Solids **156-158**, 34 (1993).
[9] W. Geertsma, J. Dijkstra, and W. van der Lugt, J. Phys. F **14**, 1833 (1984).
[10] The real space periodicity corresponding to the prepeak is $2\pi/q_P$, where q_P is the prepeak position. Due to the spherical averaging in the Fourier transform from reciprocal to direct space, the first maximum in the contribution of the prepeak to the pair distribution function will be at approximately $7.7/q_P$. For an elaborate review see, e.g. Ref. 54.
[11] H. T. J. Reijers, W. van der Lugt, and M.-L. Saboungi, Phys. Rev. B **42**, 3395 (1990).
[12] D. L. Price, M.-L. Saboungi, R. Reijers, G. Kearley, and R. White, Phys. Rev. Lett. **66**, 1894 (1991).
[13] D. L. Price and M.-L. Saboungi, Phys. Rev. B **44**, 7289 (1991).
[14] G. K. Johnson and M.-L. Saboungi, J. Chem. Phys. **86**, 6376 (1987).
[15] M.-L. Saboungi, H. T. J. Reijers, M. Blander, and G. K. Johnson, J. Chem. Phys. **89**, 5869 (1988).
[16] M. Stolz, O. Leichtweiss, R. Winter, M.-L. Saboungi, J. Fortner, and W. S. Howells, Europhys. Lett. **27**, 221 (1994).
[17] M. A. Howe and R. L. McGreevy, J. Phys. Condensed Matter **3**, 577 (1991).
[18] R. L. McGreevy and L. Pusztai, Mol. Simul. **1**, 359 (1988).
[19] R. Car and M. Parrinello, Phys. Rev. Lett. **55**, 2471 (1985).
[20] G. Seifert, G. Pastore, and R. Car, J. Phys. Condensed Matter **4**, L179 (1992).
[21] G. Galli and M. Parrinello, J. Chem. Phys. **95**, 7504 (1991).
[22] B. P. Alblas, W. van der Lugt, J. Dijkstra, W. Geertsma, and C. van Dijk, J. Phys. F **13**, 2465 (1983).
[23] S. Tamaki, T. Ishiguro, and S. Takeda, J. Phys. F **12**, 1613 (1982).
[24] C. van der Marel, P. C. Stein, and W. van der Lugt, Phys. Lett. **95**A8, 451 (1983).
[25] G. A. de Wijs, G. Pastore, A. Selloni, and W. van der Lugt, Europhys. Lett. **27**, 667 (1994).
[26] G. Pastore, E. Smargiassi, and F. Buda, Phys. Rev. A **44**, 6334 (1991).
[27] G. Galli and A. Pasquarello, *First-Principles Molecular Dynamics*, edited by M. P. Allen and D. J. Tildesley (Kluwer Academic, Dordrecht, 1993), p. 261.
[28] G. B. Bachelet, D. R. Hamann, and M. Schlüter, Phys. Rev. B **26**, 4199 (1982).
[29] I. Moullet, W. Andreoni, and P. Gianozzi, J. Chem. Phys. **90**, 7306 (1989).
[30] S. G. Louie, S. Froyen, and M. L. Cohen, Phys. Rev. B **26**, 1738 (1982).
[31] L. Kleinman and D. M. Bylander, Phys. Rev. Lett. **48**, 1425 (1982).
[32] X. Gonze, R. Stumpf, and M. Scheffler, Phys. Rev. B **44**, 8503 (1991).
[33] Q. M. Zhang, G. L. Chiarotti, A. Selloni, R. Car, and M. Parrinello, Phys. Rev. B **42**, 5071 (1990).
[34] S. Nosé, J. Chem. Phys. **81**, 511 (1984).
[35] P. E. Blöchl and M. Parrinello, Phys. Rev. B **45**, 9413 (1992).
[36] F. Tassone, F. Mauri, and R. Car, Phys. Rev. B, 50, 10 561 (1994).
[37] N. W. Ashcroft and N. D. Mermin, Solid State Physics, Saunders College, 1988.
[38] S. Baroni and P. Giannozzi, Phys. Rev. B **35**, 765 (1987).
[39] M. Buongiorno Nardelli, S. Baroni, and P. Giannozzi, Phys. Rev. Lett. **69**, 1069 (1992).
[40] A. B. Bhatia and D. E. Thornton, Phys. Rev. B **2**, 3004 (1970).
[41] F. N. Stillinger and T. A. Weber, Phys. Rev. A **25**, 978 (1982).
[42] T. A. Weber and F. H. Stillinger, Phys. Rev. B **31**, 1954 (1985).
[43] F. J. Harris, Proc. IEEE **66**, 51 (1978).
[44] K. P. Huber and G. Herzberg, *Molecular Spectra and Molecular Structure* (Van Nostrand Reinhold, New York, 1979), Vol. 4.
[45] V. E. Bondybey and J. H. English, J. Chem. Phys. **73**, 42 (1980).
[46] G. Kliche, M. Schwarz, and H.-G. von Schnering, Angew. Chem. **99**, 350 (1987).
[47] H. Bürger and R. Eujen, Z. Anorg. Allg. Chem. **394**, 19 (1972).
[48] R. R. Hart, M. B. Robin, and N. A. Kuebler, J. Chem. Phys. **42**, 3631 (1965).
[49] F. Springelkamp, R. A. de Groot, W. Geertsma, W. van der Lugt, and W. Mueller, Phys. Rev. B **32**, 2319 (1985).
[50] M. Tegze and J. Hafner, Phys. Rev. B **39**, 8263 (1989).
[51] N. F. Mott and E. A. Davis, *Electronic Processes in Non-Crystalline Materials* (Clarendon, Oxford, 1979).
[52] We assume an exponential decay of the resistivity (ρ) and use the values of ρ and $\mathrm{d}\ln(\rho)/\mathrm{d}T$ at 948 K from Ref. 5.
[53] X.-P. Li, Phys. Rev. B **41**, 8392 (1990).
[54] P. S. Salmon, Proc. R. Soc. London A Ser. **445**, 351 (1994).
[55] W. L. Slattery, G. D. Doolen, and H. E. DeWitt, Phys. Rev. A **21**, 2087 (1980).